ChemElectroChem

Research Article
doi.org/10.1002/celc.202300576

Chemistry Europe
European Chemical Societies Publishing

www.chemelectrochem.org

The Effect of Slicer Infill Pattern on the Electrochemical Performance of Additively Manufactured Electrodes

Elena Bernalte,[a] Robert D. Crapnell,[a] Ouissal M. A. Messai,[a, b] and Craig E. Banks*[a]

In this work we report the dramatic effects that changing the infill pattern has on the electrochemical performance of an additively manufactured electrode made from commercial filament. Electrodes were produced using six different slicing patterns and imaged to confirm how the infill pattern altered the working electrode surface. These electrodes were then electrochemically characterised against the near-ideal outer sphere redox probe $[Ru(NH_3)_6]^{3+}$, the common inner sphere probe $[Fe(CN)_6]^{3-}$, and then used for the electroanalytical determination of acetaminophen. It was found that changing the infill pattern had a dramatic effect on the electrochemical performance of the electrodes. Over the course of the manuscript, it can be seen that Aligned Rectilinear and Rectilinear infill patterns perform consistently well and offer good reproducibility. On the other hand, Concentric infill pattern had noticeably poor inter-electrode reproducibility and the Hilbert Curve infill was one of the worst performing electrodes in many categories. For future work in this field, we recommend the infill pattern is always reported within the experimental section to allow other researchers to repeat work properly. Additionally, when optimising an electroanalytical sensing platform, we encourage researchers to optimise the infill pattern as it has direct influence on the analytical parameters.

Introduction

Additive manufacturing, also known as 3D printing, is the general name given to a manufacturing approach in which products are made through the sequential addition of thin layers of material. The technology works through the generation of a 3D computer aided design (CAD) file, which is then processed (or sliced) into a .GCODE file that instructs the 3D printer what order to print components in. The use of a layer-by-layer approach to manufacturing, rather than more well-established subtractive or formative approaches, allows very low comparative waste generation. Additionally, the ability to print objects including complex morphologies such as nested structures and overhangs, and the continual decrease in printer size and cost means that additive manufacturing printed parts are becoming increasingly easy to print locally and on demand. The ability to print these objects in-situ, with close to zero waste, leads to significant reduction in production times and carbon footprint. These advantages over the more classical manufacturing techniques have meant the uptake of additive manufacturing within both industry and research has increased significantly.

One particular area of research that has seen a large increase in the use of additive manufacturing is within electrochemistry. Although the use of various types of additive manufacturing has been reported, such as stereolithography (SLA) and Direct Metal Laser Sintering (DMLS), Fused Filament Fabrication (FFF, also known as Fused Deposition Modelling or FDM) has proven to be the most popular. This is due to the ready availability of commercial conductive filament at a reasonable price (less than 25 p per gram) and the ability to purchase excellent FFF printers for only a few hundreds of pounds. Combined with the low-cost nature of electroanalysis, this has made FFF an attractive tool to electrochemists, allowing them to print electrodes *in-situ*, anywhere in the world. As such, there are numerous reports within the literature using commercial conductive filament for various electrochemical applications, such as for biosensor production,[1] environmental and forensic electroanalysis,[2] energy storage[3] and hydrogen generation,[4] and even the production of cells and accessories.[5] More recently, there has been a push toward the development of bespoke filaments for these applications, improving the electrochemical performance and sustainability of the approaches.[6]

Other than creating a new filament, there are various ways in which researchers have looked to improve the electrochemical performance of additively manufactured electrodes. Due to the insulating nature of the thermoplastic that makes up the majority of the filaments used within FFF, "activation" of electrodes has become common. This practice effectively removes excess thermoplastic from the surface of the printed part, or more recently filament.[7] Various methods have been reported to achieve the desired activation such as simple mechanical polishing,[8] electrochemical scanning,[2b,9] submer-

[a] Dr. E. Bernalte, Dr. R. D. Crapnell, O. M. A. Messai, Prof. Dr. C. E. Banks
Faculty of Science and Engineering, Manchester Metropolitan University,
Chester Street, Manchester, M1 5GD, United Kingdom
Tel: +44(0)1612471196
E-mail: c.banks@mmu.ac.uk

[b] O. M. A. Messai
Department of Physical Measurements, Sorbonne Paris North University,
Place du 8 Mai 1945, 93200, Saint-Denis, France

Supporting information for this article is available on the WWW under https://doi.org/10.1002/celc.202300576

sion/sonication in solvents[10] or reducing agents,[11] carbonisation,[12] thermal annealing[13] or laser-scribing.[14] These methods vary significantly and can be suited for different applications and set-ups as discussed, for more information on activation methods for additively manufactured electrodes we direct readers to Rocha and co-workers review paper.[15]

In addition to modifying the working electrodes post-print, various things can be done during the design and printing process to optimise the performance of additively manufactured electrodes. Firstly, as the filament used to produce these parts is only between 20–35 wt% conductive material (depending on source), there is significant resistance compared to an electrode produced from pure metals for example. As such, it is vital to minimise the connection length of any printed electrode to achieve the best electrochemical performance.[16] Another physical parameter alteration is the print orientation, by changing to a vertical print rather than horizontal, it has been shown that improved current values and reduced charge transfer resistance and uncompensated solution resistance can be obtained.[17] More recently, the age of the filament has been studied by Kalinke *et al.*,[18] who show that performance of additively manufactured electrodes significantly deteriorates when using older filament (up to 3 years).

There have been some published studies looking at changing individual parameters for the printing process. In terms of printing parameters it has been shown in various studies that raising the printing temperature (nozzle temperature) of the filament can result in an improvement of the electrical conductivity and electrochemical performance.[19] This has been reported to be due to an increased roughness,[19b] most likely due to being above the ideal print temperature of the material, or due to changing the conductive filler/polymer distribution within the part.[19a] It has also been shown that through optimising the printing speed used, the printed part can produce improved performance and reproducibility.[20] Various other printing parameters such as the nozzle diameter and heated bed temperature have been shown to not significantly affect the performance of additively manufactured electrodes.

One parameter yet to be investigated is the slicing pattern used when producing the .GCODE file for electrode production. In the slicing step, as mentioned above, the software takes the 3D CAD file and cuts it in consecutive pseudo-2D lines that allow the printer to construct the object. All slicing software has a default pattern that will be used to fill in the patterns produced. In the case of PrusaSlicer, an open-source slicing software, this is a rectilinear pattern which fills the voids with straight lines at 45-degree angles to each other. However, upon inspection of the printer settings section, there are numerous options available, such as concentric which would fill in a circular pattern used for working electrodes with a circular infill. The way the printer achieves the infill is of vital importance, as how the layer lines are connected will have a direct impact on the electron transfer, with increased bridged or voided areas dramatically changing performance. In this work, we look to explore how changing this infill pattern can affect the electrochemical performance of additively manufactured electrodes and offer some guidance for future research in this area.

Experimental Section

Chemicals

All chemicals used of analytical grade and were used as received without any further purification. All solutions were prepared with deionised water of resistivity not less than 18.2 MΩ cm from a Milli-Q Integral 3 system from Millipore UK (Watford, UK). Hexaaminer-uthenium (III) chloride (98%), potassium ferricyanide (III) (99%), potassium hexacyanoferrate (II) trihydrate (98.5–102.0%), sodium hydroxide (>98%), acetaminophen (98–102%) and potassium chloride (99.0–100.5%) were purchased from Merck (Gillingham, UK). Commercial conductive PLA/carbon black filament (1.75 mm, ProtoPasta, Vancouver, Canada) was purchased from Farnell (Leeds, UK).

Additive Manufacturing

All computer designs and .3MF files seen throughout this manuscript were produced using Fusion 360® (Autodesk®, CA, United States). These files were sliced and converted to .GCODE files ready for printing by the open-source software, PrusaSlicer (Prusa Research, Prague, Czech Republic). The additively manufactured electrodes (AMEs) were 3D-printed using fused filament fabrication (FFF) technology on a Prusa i3 MK3S+ (Prusa Research, Prague, Czech Republic). All AMEs were printed using a 0.6 mm nozzle with a nozzle temperature of 215 °C, 100% infill, 0.15 mm layer height, and print speed of 70 mm s^{-1}. All AME's used throughout this work were "lollipop" designs with a 5 mm disc, 10×2 mm connection stem and 1 mm thick.

Physiochemical Characterisation

Scanning Electron Microscopy (SEM) micrographs were obtained using a Crossbeam 350 Focussed Ion Beam – Scanning Electron Microscope (FIB-SEM) (Carl Zeiss Ltd., Cambridge, UK) fitted with a field emission electron gun. Imaging was completed using a Secondary Electron Secondary Ion (SESI) detector. Samples were mounted on the aluminium SEM pin stubs (12 mm diameter, Agar Scientific, Essex, UK) using adhesive carbon tabs (12 mm diameter, Agar Scientific, Essex, UK) and coated with a 3 nm layer of Au/Pd metal using a Leica EM ACE200 coating system prior to imaging.

Electrochemical Experiments

All electrochemical measurements were performed on an Autolab 100 N potentiostat controlled by NOVA 2.1.6 (Utrecht, the Netherlands). The electrochemical experiments were performed using lollipop design (Ø 5 mm, 10×2 mm connection length, 1 mm thickness) working electrodes alongside an external commercial Ag|AgCl (3 M KCl) reference electrode and a nichrome wire counter electrode. All solutions were prepared using deionised water of resistivity not less than 18.2 MΩ cm from a Milli-Q system (Merck, Gillingham, UK). All solutions of $[Ru(NH_3)_6]^{3+}$ and $[Fe(CN)_6]^{3-}$ were purged of O_2 thoroughly using N_2 prior to any electrochemical experiments.

Activation of the AMEs, when applicable, was achieved through the use of chronoamperometry as seen previously in the literature.[9a] Briefly, the AME was submerged in sodium hydroxide (0.5 M) and a

voltage of +1.4 V applied for 200 s, followed by −1.0 V for 200 s. Following this, the AME was thoroughly rinsed with deionised water and dried with compressed air.

The HET rate constants, k^0_{obs}, were calculated as an average of 3 sets of 10 different scan rates (5, 10, 15, 25, 50, 75, 100, 150, 250 and 500 mV s^{-1}), where each set used a new AME. These were performed using the near ideal outer-sphere redox probe RuHex (in 0.1 M KCl) using the well-known[21] and widely utilised Nicholson method,[22] for *quasi*-reversible electrochemical reactions *via* the following formula:[23]

$$\varphi = k^0_{obs}[\pi D n \nu F/RT]^{-1/2} \quad (1)$$

where φ is a kinetic parameter, D is the diffusion coefficient for RuHex ($D = 9.1\times10^{-6}$ cm^2 s^{-1}),[21] n is the number of electrons that are taking part in the process, F is the faraday constant, ν is the scan rate, R is the gas constant and T is the temperature in Kelvin. In order to calculate the HET rate constant, we use the peak to peak separation (ΔE_p) to deduce φ, where ΔE_p is obtained at various voltammetric scan rates.[24] The standard heterogeneous constant (k^0_{obs}) can be calculated *via* the gradient when plotting φ against $[\pi D n \nu F/RT]^{-1/2}$. In cases where ΔE_p is bigger than 212 mV, the following equation should be implemented:

$$k^0_{obs} = [\ 2.18\left(\frac{\alpha D n \nu F}{RT}\right)^{-\frac{1}{2}} \exp[-\left(\frac{\alpha \mathrm{nF}}{RT}\right)\Delta \mathrm{Ep}] \quad (2)$$

where α is assumed to be 0.5.[25]

The electroactive area of the electrode, A_{real}, is calculated using the Randles-Ševćik equation at non-standard conditions for quasi- (3) and irreversible (4) electrochemical processes when appropriate:[26]

$$I^{quasi}_{p,f} = \pm 0.436\ nFA_{real}C\ \sqrt{\frac{nFD\nu}{RT}} \quad (3)$$

$$I^{irrev}_{p,f} = \pm 0.496\ \sqrt{\alpha n'}\ nFA_{real}C\ \sqrt{\frac{nFD\nu}{RT}} \quad (4)$$

where in all cases, n is the number of electrons in the electrochemical reaction, $I_{p,f}$ is the voltammetric current (analytical signal) using the first peak of the electrochemical process, F is the Faraday constant (C mol^{-1}), ν is the applied voltammetric scan rate (V s^{-1}), R is the universal gas constant, T is the temperature in Kelvin, A_{real} is the electroactive area of the electrode (cm^2) and D is the diffusion coefficient (cm^2 s^{-1}), α is the transfer coefficient (usually assumed to be close to 0.5). Following the calculation of A_{real}, the percentage of the geometrical area was calculated using the following formula: $\%\ Real_{Area} = (A_{real}/A_{geo})\times100$. Limits of Detection (LOD) were calculated as 3 times the standard deviation of the blank (3σ) divided by the slope of the calibration plot.

Results and Discussion

Printing Patterns

To investigate the effect that solely the slicing pattern can have on the electrochemical performance of additively manufactured electrodes, an identical CAD file was used. In this case the additively manufactured electrode was designed with a 5 mm diameter and 1 mm thick disc, attached to a connection stem of 2 mm width, 10 mm length and 1 mm thickness. These files were imported into the open-source software PrusaSlicer, where they were sliced using the 6 fill patterns that were available in the top fill pattern, bottom fill pattern and general fill pattern tabs, including: Concentric, Rectilinear, Aligned Rectilinear, Archimedean Chords, Hilbert Curve, and Octagram Spiral. Only profiles that could fulfil all three types of infill were chosen although we note there are several other infill patterns available and work looking at combining different infills over one another is an area of potential future work. The slicing pattern for these profiles can be seen in Figure 1.

The electrodes were printed on identical Prusa MK3S+ 3D printers on a print bed cleaned thoroughly with isopropanol. After printing, the electrodes were examined using SEM to determine how the slicing pattern affected the electrode structure. SEM images of the top surface of the electrodes is presented in Figure 2, where significant differences in the surface finish can be seen. In all cases, there is a circular pattern with additional polymer coming from the surface, indicating the location where the print finished, and the nozzle was pulled away from the surface. It can be seen that the SEM images correlate well with the corresponding slicing patterns described in Figure 1. In all cases, a good finish was obtained with minimal gaps in the print except for the Hilbert Curve print, where due to the print head path multiple perforations were observed in the top layer. The solutions under investigation can enter these pores and ingress into the polymer matrix at a faster rate.[27] For the Concentric, Aligned Rectilinear, and Archimedean Chords prints it can be observed an increased surface roughness at the edges of the lines, indicating that there has been excess material printed causing ridges. To study whether these print styles change the electrochemical surface area or performance, we next investigated them using scan rate studies in the near-ideal outer sphere redox probe hexaaminer-uthenium (III) chloride ($[Ru(NH_3)_6]^{3+}$).

Electrochemical Characterisation

To see how these different patterns affect the electrochemical performance of the additively manufactured electrodes, initially they were investigated through a scan rate study (5–500 mV s^{-1}) using $[Ru(NH_3)_6]^{3+}$ (1 mM in 0.1 M KCl). Examples of the cyclic voltammograms obtained for the Aligned Rectilinear and Octagram Spiral prints are presented in Figure 3 A and B, with the other patterns found within Figure S1. In all cases a single reduction and oxidation peak is observed due to the one electron redox process for $[Ru(NH_3)_6]^{3+}$, however there are significant differences within the key electrochemical metrics. The cathodic peak current obtained at 25 mV s^{-1}, the peak-to-peak separation (ΔEp), the heterogeneous electrochemical rate constant (k^0_{obs}), and the electrochemical active area (A_e) are presented within Table 1, noting that the standard deviation is calculated from repeats of three separate electrodes. It can be seen that there is a significant difference between the peak reduction currents obtained using the different patterns, with Rectilinear and Aligned Rectilinear giving the largest value at

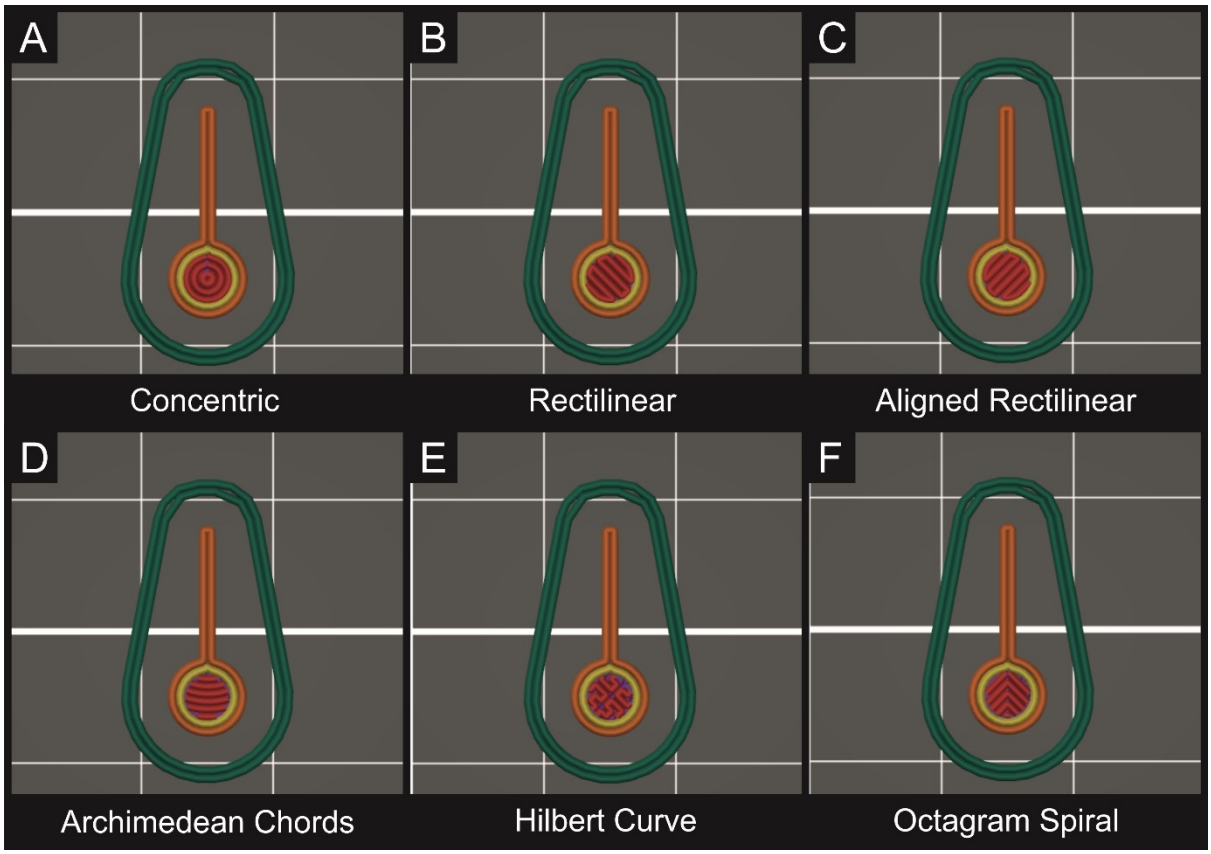

Figure 1. Images from PrusaSlicer corresponding to the slicing patterns used for each working electrode: **A)** Concentric; **B)** Rectilinear; **C)** Aligned Rectilinear; **D)** Archimedean Chords; **E)** Hilbert Curve; and **F)** Octagram Spiral.

Table 1. Comparisons of the $[Ru(NH_3)_6]^{3+}$ cathodic peak currents ($-I_p^c$), peak-to-peak separations (ΔE_p), heterogeneous electron transfer (k^0_{obs}), electrochemically active area (A_e), EIS charge transfer resistance (R_{ct}) and solution resistance (R_s) for AMEs printed using different slicer infill patterns. The uncertainties are the standard deviations across three different AME measurements.

Infill Pattern	$-I_p^c$ (μA)[a]	ΔE_p (mV)[a]	k^0_{obs} (cm s^{-1})[b]	A_e (cm^2)[b]	ΔI_p red (%)[c]	ΔI_p ox (%)[c]
Concentric	61.8 ± 3.0	255 ± 7	0.35 ± 0.02	0.44 ± 0.03	−55.2	−73.2
Rectilinear	70.9 ± 5.3	238 ± 8	0.36 ± 0.04	0.51 ± 0.04	−24.4	−46.8
Aligned Rectilinear	67.3 ± 1.6	234 ± 4	0.35 ± 0.02	0.49 ± 0.01	−18.8	−30.2
Archimedean Chords	54.7 ± 1.5	287 ± 47	0.49 ± 0.02	0.39 ± 0.11	+7.58	−18.8
Hilbert Curve	45.9 ± 1.3	272 ± 61	0.53 ± 0.03	0.32 ± 0.08	−29.4	−54.1
Octagram Spiral	64.4 ± 1.2	270 ± 12	0.43 ± 0.09	0.45 ± 0.08	+20.5	−7.92

[a]Extracted from 25 mV s^{-1} CVs in $[Ru(NH_3)_6]^{3+}$ (1 mM in 0.1 M KCl) with a nichrome wire CE and Ag | AgCl (3 M KCl) RE; [b]Calculated using cyclic voltammetry scan rate study (5–500 mV s^{-1}) in $[Ru(NH_3)_6]^{3+}$ (1 mM in 0.1 M KCl) with a nichrome wire CE and Ag | AgCl (3 M KCl) RE; Measured as the change after 100 continuous scans at 50 mV s^{-1} in $[Ru(NH_3)_6]^{3+}$ (1 mM in 0.1 M KCl) with a nichrome wire CE and Ag | AgCl (3 M KCl) RE.

25 mV s^{-1}, Figure 3C. It should be noted that the standard deviation for Rectilinear and Concentric patterns is much larger than any of the other patterns. Hilbert Curve produces the lowest reduction potential by a considerable margin, most likely due to the clear voids observed on the SEM imaging meaning there is less conductive material present. This is reflected in the values obtained for the *Ae* where again Aligned Rectilinear and Rectilinear have the largest electrochemically active area, and Hilbert Curve the lowest.

Interestingly, when analysing the *ΔEp* at slow scan rates (25 mV s^{-1}), Figure 3C, and at fast scan rates (250 mV s^{-1}), Figure 3D, there is a change. At slow scan rates Aligned Rectilinear and Rectilinear produce the smallest *ΔEp*, indicating they perform significantly better. However, at fast scan rates this swaps around considerably, leading to the case where the calculated k^0_{obs} for Hilbert Curve and Archimedean Chords are the fastest values. This indicates that when designing a system for an application, the desired speed of the measurement in addition to the sensitivities should be taken into account when

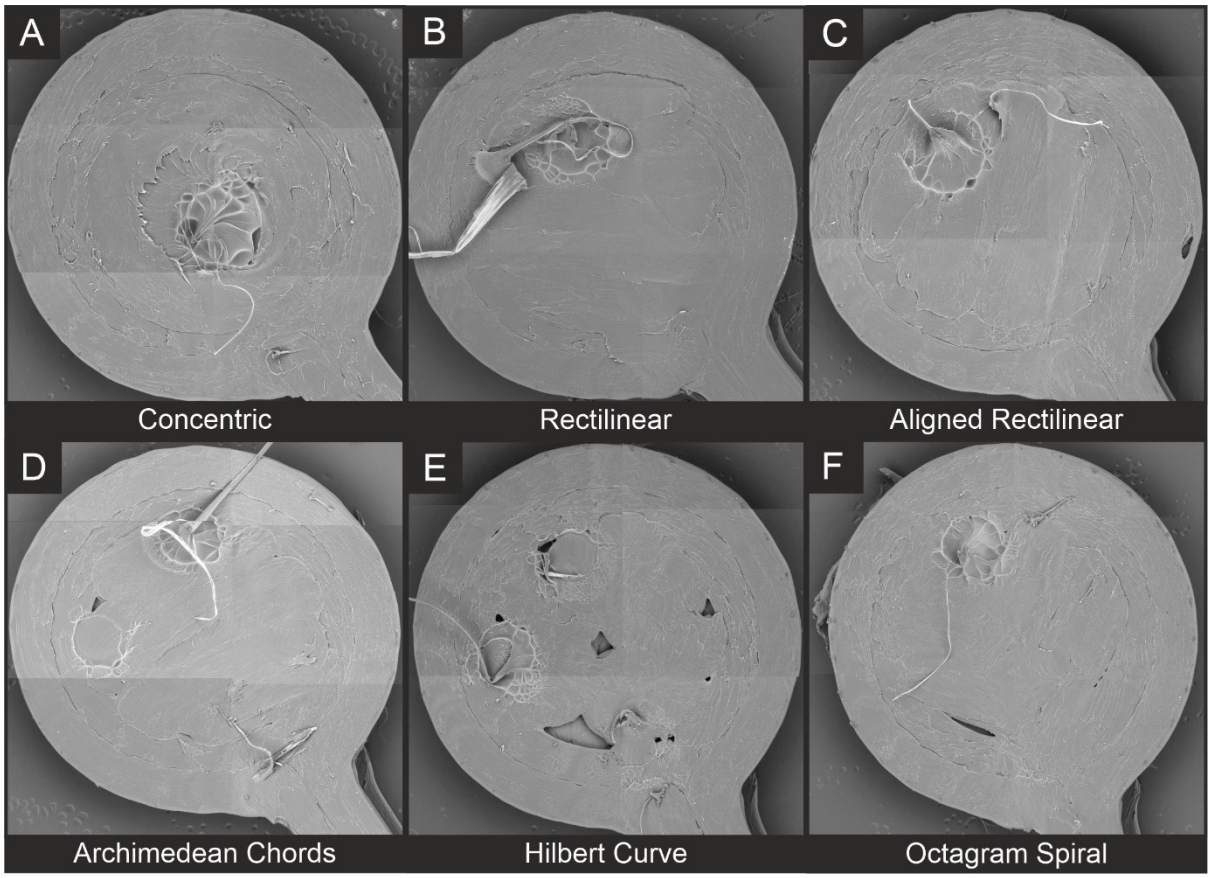

Figure 2. Combined SEM images showing the top surface of the working electrodes post-printing: **A)** Concentric; **B)** Rectilinear; **C)** Aligned Rectilinear; **D)** Archimedean Chords; **E)** Hilbert Curve; and **F)** Octagram Spiral.

choosing a slicing pattern. To further study how the changing infill pattern affects the electrochemical performance of the additively manufactured working electrodes, they were scanned 100 times using cyclic voltammetry (50 mV s^{-1}) within [Ru(NH$_3$)$_6$]$^{3+}$ (1 mM in 0.1 M KCl). The voltammograms obtained on scan 1 and scan 100 for the Aligned Rectilinear and Octagram Spiral print patterns are presented in Figure 3 E and F, respectively, with the other printing patterns shown in Figure S2. Interestingly, the peak current obtained for the reduction and oxidations processes change significantly over the course of 100 scans. In regards to the reduction current, all slicing patterns see a decrease in the peak current over the course of 100 scans, which is to be expected due to a combination of solution ingress causing a change in Ohmic drop or conductive filler surface chemistry,[27] or surface fouling of the electrode .[28] This same phenomena is observed for four of the six slicing patterns for the reduction peak, however in the case of the Archimedean Chords and Octagram Spiral prints an increase in the reduction current in observed, summarised in Table 1, of 7.58% and 20.5% respectively. More experiments are required to assess the exact reasons for this, but it is proposed that due to the nature of the Archimedean Chords and Octagram Spiral prints in the electrode surface noticed on SEM imaging, that initially the solution does not penetrate between layer lines as the gaps are so small. However, over the course of 100 scans the solution enters these pores and exposes a larger electrochemical surface area. On the other hand, for more compact prints such as Concentric there is overlap of the layer lines meaning no gaps at all and therefore only ingress occurs and more surface fouling of the electrode, meaning a reduction in electrochemical performance.

Analysis with the near-ideal outer sphere redox probe [Ru(NH$_3$)$_6$]$^{3+}$ gives valuable information about how the additively manufactured electrodes perform directly off the print bed as activation is not required to achieve a suitable electrochemical response. For use within realistic systems, such as electroanalytical sensing platforms, the analyte under consideration is more likely to be inner sphere in nature and therefore activation would be required. As such, the additively manufactured electrodes were next activated using chronoamperometry within sodium hydroxide (0.5 M vs. Ag|AgCl 3 M KCl), one of the most common activation protocols found within the literature[9a] before they were then studied using a scan rate study (5–500 mV s^{-1}) against the well-known inner sphere probe [Fe(CN)$_6$]$^{3-}$ (1 mM in 0.1 M KCl). Example of the voltammograms obtained for the Aligned Rectilinear electrode are presented in Figure 4A, with the other slicing patterns shown within Figure S3. When comparing all the slicing patterns, there is once again significant differences. Figure 4B shows example voltammograms for each slicing pattern obtained at 25 mV s^{-1}, and the

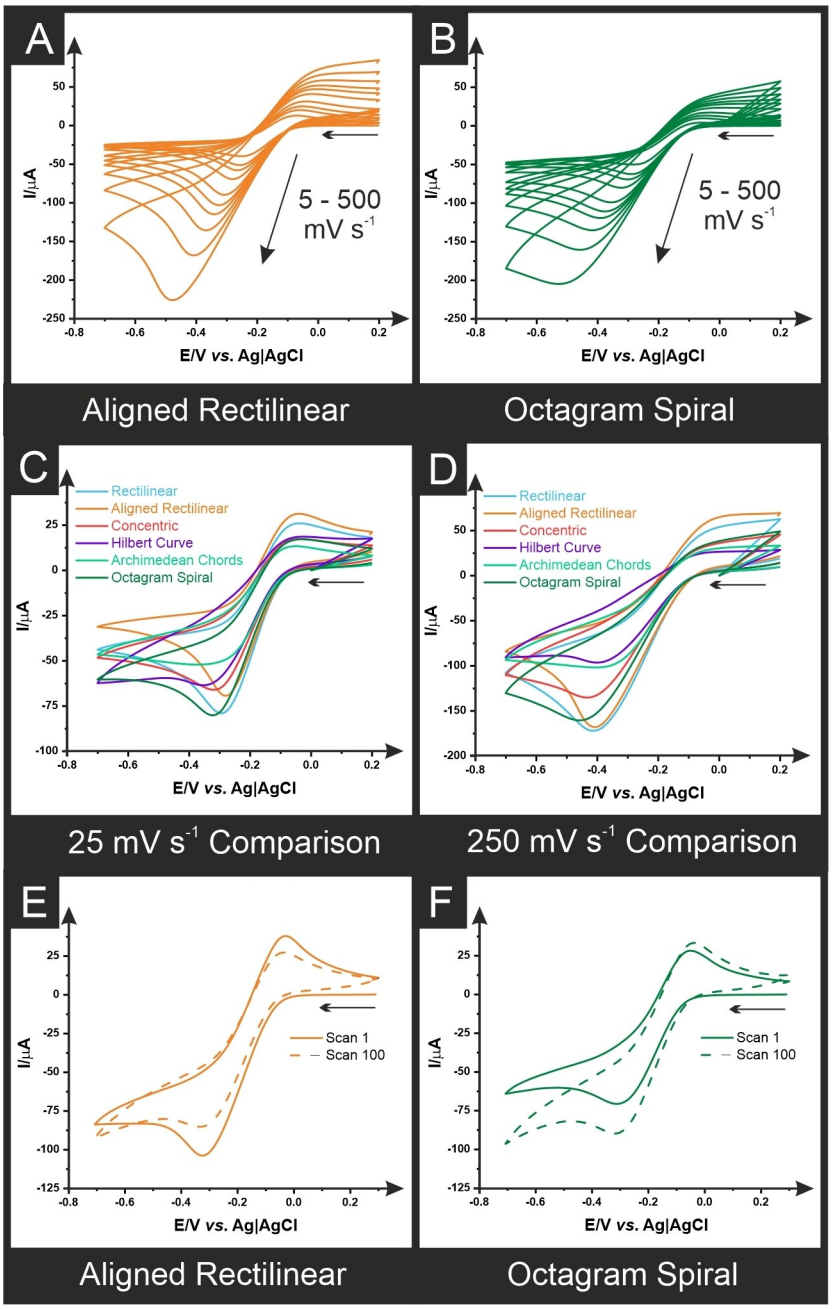

Figure 3. Example cyclic voltammograms (5–500 mV s^{-1}) from the scan rate studies using $[Ru(NH_3)_6]^{3+}$ (1 mM in 0.1 M KCl) for the **A)** Aligned Rectilinear and **B)** Octagram Spiral working electrodes. Cyclic voltammograms at **C)** 25 mV s^{-1} and **D)** 250 mV s^{-1} using $[Ru(NH_3)_6]^{3+}$ (1 mM in 0.1 M KCl) for working electrodes of all slicing patterns. Cyclic voltammograms at scan 1 and scan 100 using $[Ru(NH_3)_6]^{3+}$ (1 mM in 0.1 M KCl) for the **E)** Aligned Rectilinear and **F)** Octagram Spiral working electrodes.

key electrochemical parameters calculated from an average of three separate electrodes is presented in Table 2. It can be seen that once again the Aligned Rectilinear infill performs well in terms of current readings, giving the largest peak current of 47.4 ± 9.2 μA and a middling ΔEp of 425 ± 11 mV. In comparison, the Concentric infill performs poorly all round, offering a peak current of only 22.1 ± 9.7 μA and a ΔEp of 543 ± 88 mV. In this case, the Hilbert Cure and Octagram Spiral infill perform well in both regards, giving good peak currents and excellent ΔEp and $k_{obs}{}^{0}$ values.

Further insights into the performance of the additively manufactured working electrodes can be made from the use of Electrochemical Impedance Spectroscopy (EIS), where the solution resistance (R_s) and charge-transfer resistance (R_{CT}) can be calculated. Firstly, an electrode of each slicing pattern was subjected to 5 repeat scans of EIS within $[Fe(CN)_6]^{3-/4-}$ (1 mM in 0.1 M KCl) at frequencies between 0.1–100,000 Hz. The Nyquist plot for the 5 scans of the Aligned Rectilinear working electrode can be seen in Figure 4C, with the other infill patterns found in Figure S4. In all cases there is no significant trend in the R_s

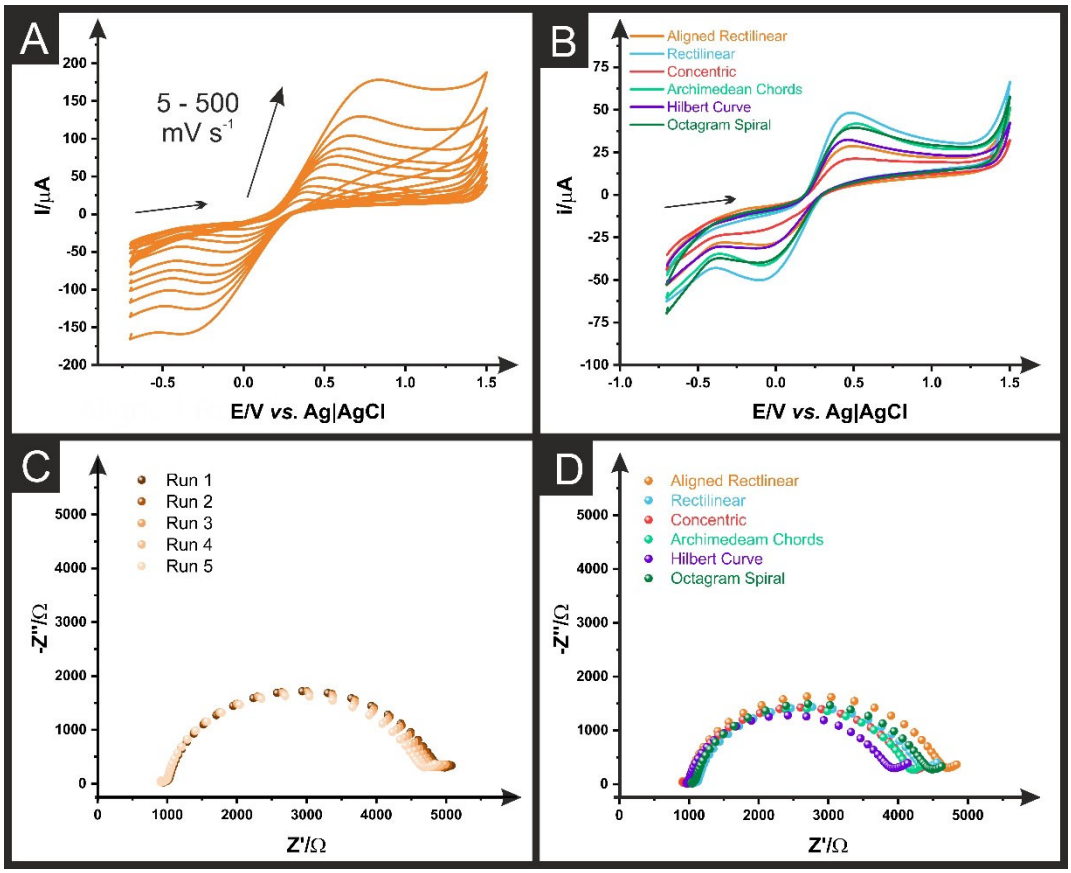

Figure 4. A) Example cyclic voltammograms (5–500 mV s^{-1}) from the scan rate studies using $[Fe(CN)_6]^{3-}$ (1 mM in 0.1 M KCl) for the Aligned Rectilinear working electrodes. **B)** Cyclic voltammograms at 25 mV s^{-1} using $[Fe(CN)_6]^{3-}$ (1 mM in 0.1 M KCl) for working electrodes of all slicing patterns. **C)** Nyquist plots from the EIS studies over 5 scans using $[Fe(CN)_6]^{3-/4-}$ (1 mM in 0.1 M KCl) for the Aligned Rectilinear working electrodes. **D)** Nyquist plots from the EIS studies 5th scan using $[Fe(CN)_6]^{3-/4-}$ (1 mM in 0.1 M KCl) for all slicing patterns.

Table 2. Comparisons of the $[Fe(CN)_6]^{3-}$ anodic peak currents ($-I_p^c$), peak-to-peak separations (ΔE_p), heterogeneous electron transfer (k^0_{obs}), electrochemically active area (A_e), EIS charge transfer resistance (R_{ct}) and solution resistance (R_s) for AMEs printed using different slicer infill patterns. The uncertainties are the standard deviations across three different AME measurements.

Infill Pattern	$-Ip^c$ (µA)[a]	ΔEp (mV)[a]	k^0_{obs} (cm s^{-1})[b]	A_e (cm^2)[b]	R_S (kΩ)[c]	R_{CT} (kΩ)[c]
Concentric	22.1 ± 9.7	543 ± 88	0.0015 ± 0.0009	0.15 ± 0.06	0.93 ± 0.04	3.19 ± 0.23
Rectilinear	25.6 ± 6.7	425 ± 11	0.0045 ± 0.0006	0.17 ± 0.04	1.05 ± 0.10	2.92 ± 0.35
Aligned Rectilinear	47.4 ± 9.2	485 ± 9	0.0033 ± 0.0006	0.32 ± 0.06	0.97 ± 0.04	3.76 ± 0.09
Archimedean Chords	39.2 ± 22	487 ± 97.2	0.0034 ± 0.0030	0.26 ± 0.15	0.98 ± 0.05	3.17 ± 0.32
Hilbert Curve	38.5 ± 9.4	426 ± 14	0.0043 ± 0.0009	0.26 ± 0.06	0.98 ± 0.10	2.97 ± 0.18
Octagram Spiral	31.2 ± 8.0	421 ± 42	0.0050 ± 0.0020	0.20 ± 0.05	0.97 ± 0.08	3.23 ± 0.08

[a]Extracted from 25 mV s^{-1} CVs in $[Fe(CN)_6]^{3-/4-}$ (1 mM in 0.1 M KCl) with a nichrome wire CE and Ag | AgCl (3 M KCl) RE; [b]Calculated using cyclic voltammetry scan rate study (5–500 mV s^{-1}) in $[Fe(CN)_6]^{3-/4-}$ (1 mM in 0.1 M KCl) with a nichrome wire CE and Ag | AgCl (3 M KCl) RE; Taken from the Nyquist plots of measurement 5 in $[Fe(CN)_6]^{3-/4-}$ (1 mM in 0.1 M KCl) with a nichrome wire CE and Ag | AgCl (3 M KCl) RE.

values over the course of 5 scans. However, for the R_{CT} values obtained from a [R(Q[RW])] fitting all show decreases sequentially through the 5 scans. Although this does not offer help in determining the best infill pattern it is of huge importance for researchers looking to create impedimetric biosensors from this commercial filament. In the case that there is significant movement in the R_{CT} values without any changes to the interface, this could result in misinterpreted results when used as a biosensor so care must be taken. It is also important to note that these phenomena may not occur on other conductive filaments so testing should be done on all new bespoke filaments produced in future. Using the 5th and most stable scan of the EIS, Nyquist plots were plotted to compare the results from each infill pattern, see Figure 4D.

The data calculated from fitting triplicates of these data with a [R(Q[RW])] fitting is also summarised in Table 2, where it

can be seen that there is no statistical difference in the R_s values obtained. In cases such as this, where the experimental set-up doesn't change other than the working electrode, the R_s can be thought of as the working electrodes internal resistance. Change can be seen in this parameter when changing the connection length, as increased resistance is added when a longer working electrode stem is used.[16] All electrodes in this study are printed with the same connection length and when observing the slicing patterns in Figure 1 and 2, it can be seen that the connection stems are printed from two straight lines. As there is no infill in this region, there is no difference between the electrodes along the connection length. However, when considering the R_{CT} there is significant differences in the fitted results. The R_{CT} results show good agreement with the k^0_{obs} data obtained from the scan rate studies, whereby the Concentric infill performs poorly, and the Hilbert Curve infill performs very well with an R_{CT} of $2.97 \pm 0.18\ k\Omega$, showing it also has good reproducibility.

Electroanalytical Application

To further test these electrodes toward a more realistic scenario, the sensing of acetaminophen (paracetamol) was studied. The successful determination of this analyte has been reported previously using additively manufactured electrodes made from this filament,[29] and therefore offers an excellent case study for observing any changes due to the infill pattern. Example cyclic voltammograms ($50\ mV\,s^{-1}$) for the detection of acetaminophen (5–240 μM in PBS pH = 7.4) for the Aligned Rectilinear and Hilbert Curve infill patterns is presented in Figure 5A and B, respectively, with the other infill patterns shown in Figure S5. It can be seen that sequential increases in the measured oxidation peak current are observed in both cases, however the Aligned Rectilinear has significantly greater magnitude. A comparison in the cyclic voltammetric response ($50\ mV\,s^{-1}$) for the detection of acetaminophen (40 μM in PBS pH = 7.4) for all infill patterns is shown within Figure 5C, where it can be seen that there are significant differences in the peak shape, the peak potential and the peak current for the oxidation of acetaminophen. This correlates with the calibration plots for each infill pattern shown within Figure 5D, which were used to calculate the important electroanalytical parameters such as sensitivity, limit of quantification (LOQ) and limit of detection (LOD), where the LOQ and LOD are calculated by 10σ/b and 3σ/b, respectively, with σ being the standard deviation of the blank and b being the gradient of the slope from the calibration plot. These calculated key parameters are summarised in Table 3.

It can be seen that there are significant differences across all calculated parameters. Hilbert Curve and Octagram Spiral infill

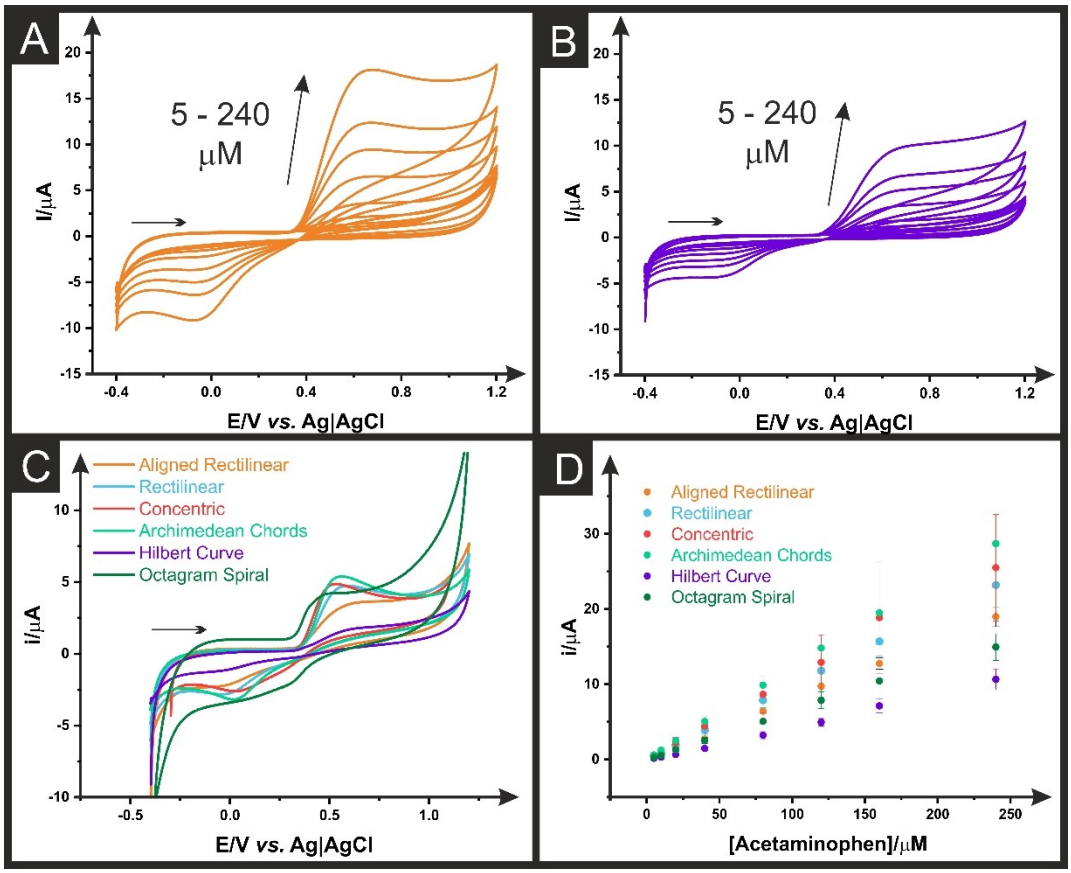

Figure 5. Example cyclic voltammograms ($50\ mV\,s^{-1}$) for the detection of acetaminophen (5–240 μM in PBS pH = 7.4) for the **A)** Aligned Rectilinear and **B)** Hilbert Curve working electrodes. **C)** Cyclic voltammograms ($50\ mV\,s^{-1}$) for the detection of acetaminophen (40 μM in PBS pH = 7.4) for working electrodes of all slicing patterns. **D)** Calibration plots for the detection of acetaminophen (5–240 μM in PBS pH = 7.4) for the working electrodes of all slicing patterns.

Table 3. Comparisons of the sensitivity, limit of quantification (LOQ), limit of detection (LOD) and recoveries for the detection of acetaminophen using AMEs printed using different slicer infill patterns. The sensitivity, limit of quantification (LOQ) and limit of detection (LOD) are calculated from results in PBS (pH = 7.4). The uncertainties are the standard deviations across three different AME measurements.

Infill Pattern	Sensitivity ($\mu A\,\mu M^{-1}$)	LOQ (μM)	LOD (μM)
Concentric	0.109 ± 0.003	24.2 ± 0.64	7.3 ± 0.2
Rectilinear	0.097 ± 0.001	4.62 ± 0.03	1.39 ± 0.01
Aligned Rectilinear	0.080 ± 0.001	7.24 ± 0.05	2.17 ± 0.02
Archimedean Chords	0.120 ± 0.001	12.3 ± 0.14	3.69 ± 0.04
Hilbert Curve	0.045 ± 0.001	16.5 ± 0.24	4.97 ± 0.07
Octagram Spiral	0.063 ± 0.001	26.1 ± 0.39	7.84 ± 0.12

patterns perform badly across the board, with low sensitivities, high LOQ and LOD, and poor standard deviations between electrodes. The Concentric pattern gave impressive sensitivities but had a large deviation between electrodes, meaning its LOQ and LOD were poor, this highlights how irreproducible this infill pattern is. The two patterns that performed the most consistently across the board for the electroanalytical approach is the Rectilinear and Aligned Rectilinear infill patterns, with the Rectilinear performing slightly better with a sensitivity of $0.097 \pm 0.001\ \mu A\,\mu M^{-1}$, a LOQ of $4.62 \pm 0.03\ \mu M$ and a LOD of $1.39 \pm 0.01\ \mu M$. When compared to the values obtained for the Octagram Spiral infill pattern with a sensitivity of $0.063 \pm 0.001\ \mu A\,\mu M^{-1}$, a LOQ of $26.1 \pm 0.39\ \mu M$ and a LOD of $7.84 \pm 0.12\ \mu M$, it can be seen how large the effect slicing infill pattern has on the final performance of an additively manufactured electroanalytical device. Due to the advantages additive manufacturing has over other manufacturing methodologies mentioned earlier, we predict that its use within electrochemistry will continue to rise. We therefore recommend when applying additively manufactured electrochemical platforms the infill pattern is always reported within the experimental section to allow other researchers to reproduce the experimental observations. Additionally, when optimising an electroanalytical sensing platform, it would be important to find the most adequate infill pattern for the specific application too.

Conclusions

In conclusion, this work demonstrates the large changes in electrochemical performance that are seen when changing the infill pattern for identical additively manufactured working electrodes. The electrodes were first imaged under SEM to highlight the change in surface structure obtained when changing the infill. The electrochemical performance was evidenced through scan rate studies within the near-ideal outer sphere redox probe $[Ru(NH_3)_6]^{3+}$, the common inner sphere probe $[Fe(CN)_6]^{3-}$. This allowed for the calculations of the heterogeneous electrochemical rate constant and the electrochemically active area, which showed significant differences between the infill patterns. This was then shown for the electroanalytical determination of acetaminophen within buffered solutions, where again large variations were seen. Throughout the manuscript, it was seen that Aligned Rectilinear and Rectilinear infill patterns perform consistently well and offer good reproducibility. It is noted that the Concentric infill pattern had noticeably poor inter-electrode reproducibility and the Hilbert Curve infill was one of the worst performing electrodes in many categories. For future work in this field, we recommend the infill pattern is always reported within the experimental section of the work to allow other researchers to repeat work properly. Additionally, when optimising an electroanalytical sensing platform, it would be wise to optimise the infill pattern.

Supporting Information

The Supporting Information is available free of charge. Cyclic voltammograms of $[Ru(NH_3)_6]^{3+}$ and $[Fe(CN)_6]^{3-}$, EIS measurements and the cyclic voltammograms of acetaminophen.

Acknowledgements

The authors would like to thank Dr. Hayley Andrews for collecting SEM data. We thank EPSRC for funding (EP/W033224/1).

Conflict of Interests

The authors declare no conflict of interest.

Data Availability Statement

The data that support the findings of this study are available in the supplementary material of this article.

Keywords: Additive manufacturing · fused filament fabrication · electrochemistry · printing parameters · electroanalysis

[1] a) C. Kalinke, R. D. Crapnell, E. Sigley, M. J. Whittingham, P. R. de Oliveira, L. C. Brazaca, B. C. Janegitz, J. A. Bonacin, C. E. Banks, *Chem. Eng. J.* **2023**, *467*, 143513; b) J. Muñoz, M. Pumera, *TrAC Trends Anal. Chem.* **2020**, *128*, 115933.
[2] a) I. V. Arantes, R. D. Crapnell, M. J. Whittingham, E. Sigley, T. R. Paixão, C. E. Banks, *ACS Appl. Eng. Mater.* **2023**; b) H. M. Elbardisy, E. M. Richter, R. D. Crapnell, M. P. Down, P. G. Gough, T. S. Belal, W. Talaat, H. G. Daabees, C. E. Banks, *Anal. Methods* **2020**, *12*, 2152–2165; c) B. C. Janegitz, R. D. Crapnell, P. Roberto de Oliveira, C. Kalinke, M. J. Whittingham, A. Garcia-Miranda Ferrari, C. E. Banks, *ACS Meas. Sci. Au* **2023**.
[3] a) P. Wuamprakhon, R. D. Crapnell, E. Sigley, N. J. Hurst, R. J. Williams, M. Sawangphruk, E. M. Keefe, C. E. Banks, *Adv. Sustainable Syst.* **2023**, *7*, 2200407; b) P. Chang, H. Mei, S. Zhou, K. G. Dassios, L. Cheng, *J. Mater. Chem. A* **2019**, *7*, 4230–4258; c) C. W. Foster, M. P. Down, Y. Zhang, X. Ji, S. J. Rowley-Neale, G. C. Smith, P. J. Kelly, C. E. Banks, *Sci. Rep.* **2017**, *7*, 42233.
[4] a) J. P. Hughes, P. L. dos Santos, M. P. Down, C. W. Foster, J. A. Bonacin, E. M. Keefe, S. J. Rowley-Neale, C. E. Banks, *Sustain. Energy Fuels* **2020**, *4*, 302–311; b) C. Iffelsberger, S. Ng, M. Pumera, *Appl. Mater. Today* **2020**, *20*, 100654; c) K. A. Kumar, K. Ghosh, O. Alduhaish, M. Pumera, *Electrochem. Commun.* **2021**, *122*, 106890.
[5] M. J. Whittingham, R. D. Crapnell, E. J. Rothwell, N. J. Hurst, C. E. Banks, *Talanta Open* **2021**, *4*, 100051.
[6] a) I. V. Arantes, R. D. Crapnell, E. Bernalte, M. J. Whittingham, T. R. Paixão, C. E. Banks, *Anal. Chem.* **2023**; b) R. D. Crapnell, I. V. Arantes, M. J. Whittingham, E. Sigley, C. Kalinke, B. C. Janegitz, J. A. Bonacin, T. R. Paixão, C. E. Banks, *Green Chem.* **2023**; c) R. D. Crapnell, E. Sigley, R. J. Williams, T. Brine, A. Garcia-Miranda Ferrari, C. Kalinke, B. C. Janegitz, J. A. Bonacin, C. E. Banks, *ACS Sustainable Chem. Eng.* **2023**; d) E. Sigley, C. Kalinke, R. D. Crapnell, M. J. Whittingham, R. J. Williams, E. M. Keefe, B. C. Janegitz, J. A. Bonacin, C. E. Banks, *ACS Sustainable Chem. Eng.* **2023**, *11*, 2978–2988.
[7] R. S. Shergill, B. A. Patel, *ACS Appl. Electron. Mater.* **2023**, *5*, 5120–5128.
[8] C. Kalinke, N. V. Neumsteir, G. de Oliveira Aparecido, T. V. de Barros Ferraz, P. L. Dos Santos, B. C. Janegitz, J. A. Bonacin, *Analyst* **2020**, *145*, 1207–1218.
[9] a) E. M. Richter, D. P. Rocha, R. M. Cardoso, E. M. Keefe, C. W. Foster, R. A. Munoz, C. E. Banks, *Anal. Chem.* **2019**, *91*, 12844–12851; b) D. P. Rocha, C. W. Foster, R. A. Munoz, G. A. Buller, E. M. Keefe, C. E. Banks, *Analyst* **2020**, *145*, 3424–3430.
[10] R. Gusmão, M. P. Browne, Z. Sofer, M. Pumera, *Electrochem. Commun.* **2019**, *102*, 83–88.
[11] E. Redondo, J. Muñoz, M. Pumera, *Carbon* **2021**, *175*, 413–419.
[12] E. Redondo, S. Ng, J. Muñoz, M. Pumera, *Nanoscale* **2020**, *12*, 19673–19680.
[13] F. Novotný, V. Urbanová, J. Plutnar, M. Pumera, *ACS Appl. Mater. Interfaces* **2019**, *11*, 35371–35375.
[14] D. P. Rocha, V. N. Ataide, A. de Siervo, J. M. Gonçalves, R. A. Muñoz, T. R. Paixão, L. Angnes, *Chem. Eng. J.* **2021**, *425*, 130594.
[15] D. P. Rocha, R. G. Rocha, S. V. Castro, M. A. Trindade, R. A. Munoz, E. M. Richter, L. Angnes, *Electrochem. Sci. Advances* **2021**, e2100136.
[16] R. D. Crapnell, A. Garcia-Miranda Ferrari, M. J. Whittingham, E. Sigley, N. J. Hurst, E. M. Keefe, C. E. Banks, *Sensors* **2022**, *22*, 9521.
[17] a) H. H. Bin Hamzah, O. Keattch, D. Covill, B. A. Patel, *Sci. Rep.* **2018**, *8*, 9135; b) A. Abdalla, H. Hamzah, O. Keattch, D. Covill, B. Patel, *Electrochim. Acta* **2020**, *354*, 136618.
[18] C. Kalinke, P. R. de Oliveira, N. V. Neumsteir, B. F. Henriques, G. de Oliveira Aparecido, H. C. Loureiro, B. C. Janegitz, J. A. Bonacin, *Anal. Chim. Acta* **2021**, 339228.
[19] a) C. Iffelsberger, C. W. Jellett, M. Pumera, *Small* **2021**, 2101233; b) R. S. Shergill, C. L. Miller, B. A. Patel, *Sci. Rep.* **2023**, *13*, 339.
[20] R. S. Shergill, B. A. Patel, *ChemElectroChem* **2022**, *9*, e202200831.
[21] A. García-Miranda Ferrari, C. W. Foster, P. Kelly, D. C. Brownson, C. E. Banks, *Biosensors* **2018**, *8*.
[22] R. S. Nicholson, *Anal. Chem.* **1965**, *37*, 1351–1355.
[23] S. J. Rowley-Neale, D. A. C. Brownson, C. E. Banks, *Nanoscale* **2016**, *8*, 15241–15251.
[24] D. Brownson, C. E. Banks, *The Handbook of Graphene Electrochemistry*, Springer London, **2014**.
[25] a) F. E. Galdino, C. W. Foster, J. A. Bonacin, C. E. Banks, *Anal. Methods* **2015**, *7*, 1208–1214; b) C. W. Foster, M. P. Down, Y. Zhang, X. Ji, S. J. Rowley-Neale, G. C. Smith, P. J. Kelly, C. E. Banks, *Sci. Rep.* **2017**, *7*, 42233.
[26] A. Bard, L. Faulkner, *Electrochemical Methods: Fundamentals and Applications*, John Wiley & Sons, Inc, Chichester, **2001**.
[27] R. J. Williams, T. Brine, R. D. Crapnell, A. G.-M. Ferrari, C. E. Banks, *Mater. Adv.* **2022**, *3*, 7632–7639.
[28] B. L. Hanssen, S. Siraj, D. K. Wong, *Rev. Anal. Chem.* **2016**, *35*, 1–28.
[29] R. D. Crapnell, E. Bernalte, A. G.-M. Ferrari, M. J. Whittingham, R. J. Williams, N. J. Hurst, C. E. Banks, *ACS Measurement Science Au* **2021**, *2*, 167–176.

Manuscript received: October 20, 2023
Revised manuscript received: December 1, 2023
Version of record online: ■■, ■■

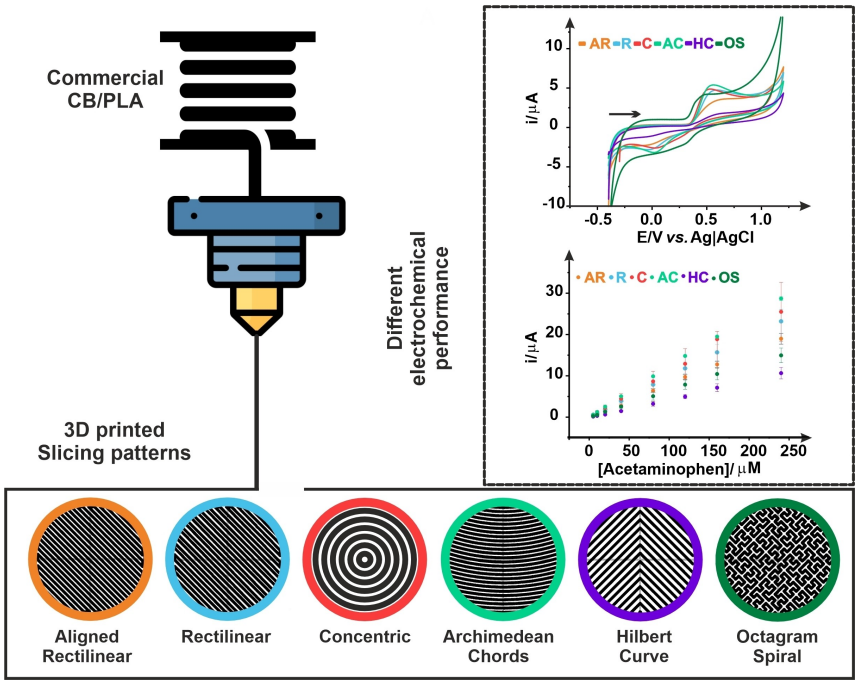

This work presents the extraordinary differences that can be obtained in the electrochemical performance of additively manufactured electrodes when simply changing the infill pattern style within the slicing software.

*Dr. E. Bernalte, Dr. R. D. Crapnell, O. M. A. Messai, Prof. Dr. C. E. Banks**

1 – 11

The Effect of Slicer Infill Pattern on the Electrochemical Performance of Additively Manufactured Electrodes